Observation of a Critical Gradient Threshold for Electron Temperature Fluctuations in the DIII-D Tokamak

J. C. Hillesheim, J. C. DeBoo, W. A. Peebles, T. A. Carter, G. Wang, T. L. Rhodes, L. Schmitz, G. R. McKee, Z. Yan, G. M. Staebler, K. H. Burrell, E. J. Doyle, C. Holland, C. C. Petty, S. P. Smith, A. E. White, and L. Zeng

Phys. Rev. Lett. **110**, 045003 — Published 23 January 2013

DOI: 10.1103/PhysRevLett.110.045003

Observation of a critical gradient threshold for electron temperature fluctuations in the DIII-D tokamak

J. C. Hillesheim,[1, a)] J. C. DeBoo,[2] W. A. Peebles,[1] T. A. Carter,[1] G. Wang,[1] T. L. Rhodes,[1] L. Schmitz,[1] G. R. McKee,[3] Z. Yan,[3] G. M. Staebler,[2] K. H. Burrell,[2] E. J. Doyle,[1] C. Holland,[4] C. C. Petty,[2] S. P. Smith,[2] A. E. White,[5] and L. Zeng[1]

[1)] *Department of Physics and Astronomy, University of California, Los Angeles, Los Angeles, California 90024-1547, USA*

[2)] *General Atomics, San Diego, California 92186-5608, USA*

[3)] *University of Wisconsin, Madison, Madison, Wisconsin 53706-1687, USA*

[4)] *University of California, San Diego, La Jolla, California 92093-0417, USA*

[5)] *Massachusetts Institute of Technology, Cambridge, Massachusetts 02139, USA*

A critical gradient threshold has been observed for the first time in a systematic, controlled experiment for a locally measured turbulent quantity in the core of a confined high-temperature plasma. In an experiment in the DIII-D tokamak where $L_{T_e}^{-1} = |\nabla T_e|/T_e$ and toroidal rotation were varied, long wavelength ($k_\theta \rho_s \lesssim 0.4$) electron temperature fluctuations exhibit a threshold in $L_{T_e}^{-1}$: below they change little, above they steadily increase. The increase in $\delta T_e/T_e$ is concurrent with increased electron heat flux and transport stiffness. Observations were insensitive to rotation. Accumulated evidence strongly enforces the identification of the experimentally observed threshold with ∇T_e-driven trapped electron mode turbulence.

PACS numbers: 52.35.Ra, 52.55.Fa, 52.70.Gw, 52.25.Fi

[a)] Electronic mail: jchillesheim@physics.ucla.edu

Plasma turbulence plays a major role in redistributing energy in a broad array of physical systems, such as astrophysical[1], processing[2], and laboratory plasmas[3], including the hot, confined plasmas used for fusion energy research. This is particularly true for magnetic confinement fusion devices, where the transport of particles, momentum, and heat across the magnetic field by gyroradius-scale turbulence is a major issue. This turbulence is widely thought to arise due to linear instabilities, differing from neutral fluid dynamics, where turbulence arises while the system is linearly stable[4]. Many of these gyroradius-scale modes are expected to exhibit a threshold in the equilibrium gradient providing free energy for the instability, where the mode is linearly stable below the threshold and unstable above[5]. Direct, systematic observation of instability has been related to critical gradient criteria in linear experiments[6–8]; however, no previous work exists in the core of a confined high-temperature plasma. Indirect evidence supporting the existence of critical gradients has been reported in tokamaks for both electron and ion thermal transport[9–13]. Many experiments in tokamaks have related fluctuation levels monotonically to driving gradients or input power, or investigated transient measurements[3], but controlled, steady-state observations directly demonstrating a threshold for a gradient in a systematic experiment have proven elusive due to the combination of plasma conditions, localized heating, and diagnostic capabilities necessary to isolate and directly observe the critical gradient behavior. A generic attribute of gradient-driven turbulence is that the system tends to be constrained nearby the marginal value for the critical gradient. The dynamics of this process have been studied, for instance, within the context of self-organized criticality[14] for plasma turbulence[15]. We present observations of how linear stability, measured fluctuations, and heat flux are related as a critical gradient is surpassed in a toroidal, high temperature plasma.

A phenomenon related to critical gradients is stiff transport. Qualitatively, stiffness locally parameterizes the incremental change in flux for an incremental change in gradient. A consequence of globally stiff transport (*i.e.* high stiffness at all radii) is little change to equilibrium profiles with additional source input. Since fusion power in a magnetically confined plasma is proportional to pressure squared, the diminishing returns enforced by stiff

heat transport could present an issue for the efficiency of future reactors[16]. The observations presented here relate to electron temperature fluctuations and local profile stiffness, which is relevant to scenarios with strong electron heating, such as would be expected by alpha particles in burning plasmas.

In this Letter, for the first time, we present direct, systematic evidence of a critical gradient threshold in a locally measured turbulence characteristic in the core of a tokamak. As illustrated in Fig. 1(a), we observe a threshold in $L_{T_e}^{-1} = |\nabla T_e|/T_e$[17] above which electron temperature fluctuations, $\delta T_e/T_e$, steadily increase. A critical gradient was simultaneously observed for electron thermal transport, the effect of which can be seen in Fig. 1(b). In contrast, measurements of the density fluctuation level have no definite threshold.

The experiment was performed in the DIII-D tokamak[18] and was designed to investigate critical gradients and electron profile stiffness[19]. Plasmas were in L-mode (no edge transport barrier), MHD-quiescent (no equilibrium-scale instabilities impacted the presented measurements), upper single null diverted (magnetic geometry with a single magnetic X-point, at the top of the plasma), with plasma current $I_p = 0.8$ MA, minor radius $a \approx 0.6$ m, major radius $R_0 \approx 1.7$ m, $B_0 = 2$ T toroidal magnetic field (directed opposite to I_p), and had line-averaged density of $\sim 2 \times 10^{13}$ cm^{-3}. The resonance locations of six gyrotrons used for electron cyclotron heating (ECH) were switched shot-to-shot between $\rho = 0.5$ and $\rho = 0.7$, which scanned $L_{T_e}^{-1}$ at $\rho = 0.6$, as shown in Fig. 2. In addition to ECH-only cases, neutral beam injection (NBI) was employed to investigate the $L_{T_e}^{-1}$ scans for three rotation conditions: two co-injected (same direction as I_p) NBI sources (ECH+Co-NBI), two counter-injected NBI sources (ECH+Ctr-NBI), and balanced injection with one of each (ECH+Bal-NBI). Combinations of NBI and ECH were held in steady-state for 500-800 ms. These steady-state time periods were used to average profile and turbulence measurements. One ECH source was modulated at 50% duty cycle for transient heat pulse analysis; this had a neglible effect on the turbulence measurements. There was ~ 3 MW ECH power in all shots. NBI periods had ~ 2 MW of beam power.

Figure 2 shows the response of the equilibrium T_e and $L_{T_e}^{-1}$ profiles to ECH location for

the ECH-only case. The change in $L_{T_e}^{-1}$ was predominantly due to ∇T_e; T_e also increased, but was restricted to the range of 0.7 to 0.9 keV at $\rho = 0.6$. The local value of $L_{T_e}^{-1}$ from data as in Fig. 2 provides the abscissa value for each $\delta T_e/T_e$ measurement in Fig. 1. There are $\sim 25\%$ uncertainties in plotted values of $L_{T_e}^{-1}$.

The n_e profiles and T_e profiles for $\rho > 0.5$ were well-matched (to each other) for all conditions; although, the minimum value of $L_{T_e}^{-1}$ for cases with NBI were higher. The T_i profiles were well-matched for cases with NBI, but were uniformly lower for ECH-only. The effective ionic charge at $\rho \approx 0.6$ for most of the discharges was $Z_{eff} \approx 2.3 - 2.8$, but was systematically higher for shots with ECH+Ctr-NBI, where $Z_{eff} \approx 2.9 - 3.2$. The main ion species was deuterium and the dominant impurity was carbon. The presented results indicate little sensitivity to toroidal rotation and flow shear changes.

Simultaneous measurements of $\delta T_e/T_e$ and the crossphase, α_{n_e,T_e}, between electron temperature and density fluctuations were acquired with a coupled correlation electron cyclotron emission (CECE) radiometer and reflectometer[20–22]. The CECE system[23] acquired $\delta T_e/T_e$ at two radial locations, $\rho \approx 0.55$ and $\rho \approx 0.61$; the plasma was optically thick ($\tau > 5$) for the ECE measurements. A reflectometer array[24] overlapped the CECE channels at $\rho \approx 0.61$; most shots also showed significant, though lower, coherency with CECE channels at $\rho \approx 0.55$. Due to small density profile variations, there existed some mismatch in the radial location of the closest CECE and reflectometer channels; however, this would be expected to only change the measured coherency, not the crossphase[21]. Beam emission spectroscopy[25] (BES) measured density fluctuations, $\delta n/n$, during the ECH+Co-NBI case. All reported turbulence measurements are long wavelength ($k_\theta \rho_s \lesssim 0.5$, ρ_s is the ion sound gyroradius and k_θ is the poloidal wavenumber).

The principal result is shown in Fig. 1, where both the local electron heat flux and $\delta T_e/T_e$ increase rapidly above a critical value of $L_{T_e}^{-1}$. Figure 1(a) shows $\delta T_e/T_e$ measurements: a threshold value is observed at $L_{T_e}^{-1} \approx 3$ m^{-1}, below which $\delta T_e/T_e$ is constant (within uncertainties, given by the detection limit of the diagnostic[21,26]), and above which it steadily increases by a factor of ~ 2. This observation is consistent with the trapped electron mode

(TEM) instability[27] that is characterized by growth rates proportional to $L_{T_e}^{-1}$. The normalized collision frequency, $\nu^* = \nu_{ei}/(c_s/a)$ (ν_{ei} is the electron-ion collision frequency), is ~ 0.1 at the measurement locations and β (ratio of plasma pressure to magnetic field pressure) is $< 0.5\%$, which places the experiment in a TEM relevant regime. The electron heat flux from power balance analysis for the data set is plotted in Fig. 1(b), normalized to the gyro-Bohm flux (the expected scale size of the flux from dimensional analysis), $Q_{GB} = n_e T_e c_s (\rho_s/a)^2$, where $c_s = \sqrt{T_e/m_i}$. The heat flux increases nonlinearly with $L_{T_e}^{-1}$, similar to Ref. 11. The electron heat flux inferred by power balance transport analysis is heavily-constrained by the heat sources; varying input profiles within uncertainties yields an estimated random error of $\sim 5\%$ or less. Systematic errors would be expected to be highly-correlated and should not affect interpretations of results. For further transport analysis and equilibrium information, including quantification of stiffness, see Ref. 19.

Measurements of $\delta n/n$ from BES, depicted in Fig. 1(a), at $\rho \approx 0.58$ in the ECH+Co-NBI scan show a $\sim 25\%$ increase from the minimum $L_{T_e}^{-1}$ to the next lowest value, above which $\delta n/n$ shows little change. The increase in the ratio $(\delta T_e/T_e)/(\delta n/n)$ is consistent with a transition to predominantly TEM turbulence[28].

Model fits were performed to quantify the threshold value. Taking the electron thermal diffusivity, χ_e, to be proportional to $(\delta T_e/T_e)^2$ and using a functional form similar to Ref. 29, the $(\delta T_e/T_e)^2$ data was fit to

$$c_0 + c_1 \left(L_{T_e}^{-1} - L_{T_e}^{-1}|_{crit}\right)^{\ell} H\left(L_{T_e}^{-1} - L_{T_e}^{-1}|_{crit}\right), \tag{1}$$

where $H(x)$ is the Heaviside function and c_0, c_1, l, and $L_{T_e}^{-1}|_{crit}$ are the fit parameters. By varying $(\delta T_e/T_e)^2$ within uncertainties, the average and standard deviation of an ensemble of fits resulted in $L_{T_e}^{-1}|_{crit} = 2.8 \pm 0.4\ \mathrm{m}^{-1}$. The average fit is shown with a solid line in Fig. 1(a). Several functional forms were used, with Eq. 1 yielding the smallest average goodness-of-fit parameter, χ^2, for the ensemble.

A critical gradient for χ_e was also found for ECH-only plasmas using transient heat pulse analysis[19] at $L_{T_e}^{-1}|_{crit} \approx 3.0 \pm 0.2\ \ \mathrm{m}^{-1}$, which is within uncertainties of the critical value for

$\delta T_e/T_e$. Above the threshold, stiffness locally increased, as reflected in Fig. 1(b).

It has been argued in previous work that zonal flows have little influence on ∇T_e-TEM turbulence, with little expected non-linear upshift of the critical gradient[30,31]. The experimental results are therefore compared to linear predictions and we defer detailed comparison to nonlinear simulations to future work. Figure 3(a) shows linear gyrofluid results from the code TGLF[32], which use experimental profiles for inputs. Globally, density profiles were well-matched from shot-to-shot, but small variations in the local density gradient appear to be significant. Plotted is the mean growth rate over $0.0 \leq k_\theta \rho_s \leq 0.4$ of the fastest growing mode propagating in the electron diamagnetic direction, $\langle \gamma_e/(c_s/a) \rangle$, where the upper bound was chosen to approximate the CECE diagnostic. The remaining scatter in the data is attributed to additional dependencies beyond η_e. A rapid increase begins at $\eta_e \approx 2$, consistent with critical gradient behavior. Figure 3(b) shows the $\delta T_e/T_e$ data in Fig. 1(b) plotted as a function of η_e; a sharp increase occurs at $\eta_e \approx 1.9$.

Figure 4(a) shows measured $\delta T_e/T_e$ power spectra in the ECH+Bal-NBI case: the measured fluctuation level increases with $L_{T_e}^{-1}$. Values for $\delta T_e/T_e$ plotted in Fig. 1 are determined by integration of the $\delta T_e/T_e$ power spectra between 0-400 kHz. The peaks at ~ 20 kHz in Fig. 4(a) appear to be related to a geodesic acoustic mode. Fig. 4(b) shows the coherency between electron temperature and density fluctuations; note, since thermal noise determined by the equilibrium value of T_e dominates the autopower spectrum of a single ECE channel, one would expect the coherency to increase if $\delta T_e/T_e$ increases, all else the same. A large number of records are used, $\sim 2\text{k} - 4\text{k}$ from the long steady-state periods, so even coherency values of $\gamma_{n_e,T_e} \approx 0.05 - 0.10$ are significant. For the other conditions in the rotation scan, the peak in the spectra that occurs at ~ 80 kHz in Fig. 4(b) shifts, consistent with a Doppler shift due to the equilibrium $E \times B$ drift, which is dominated by toroidal rotation. Figure 4(c) shows the crossphase associated with Fig. 4(b): α_{n_e,T_e} increases ($\widetilde{n}_e$ and $\widetilde{T}_e$ more in-phase, $\widetilde{n}_e$ leads $\widetilde{T}_e$) with $L_{T_e}^{-1}$. A relatively constant crossphase is measured over frequencies with sufficiently high coherency.

Values for α_{n_e,T_e} are plotted in Fig. 5, averaged over the frequency range where $\gamma_{n_e,T_e} \geq$

80% of the maximum coherency. The crossphase between fields is a fundamental property of the linear modes driving the turbulence and large modifications to its value imply a change of the dominant instability. Figure 5 shows that the measured crossphase in the four heating scenarios converge at high $L_{T_e}^{-1}$, implying that a single common mode is present in all cases. In contrast, the crossphase below the threshold differs significantly, implying different instabilities. Within each NBI configuration α_{n_e,T_e} changes with $L_{T_e}^{-1}$ while rotation and flow shear did not vary significantly. Additionally, different rotation and shear values correspond to several of the same α_{n_e,T_e} values. This shows α_{n_e,T_e} is not directly dependent on rotation or flow shear in this experiment; similar reasoning applies to the $\delta T_e/T_e$ measurements.

For the $L_{T_e}^{-1}$ scans in ECH+Co-NBI and ECH+Bal-NBI, the trends and values in crossphase are remarkably similar to previous experiments[21,22,33,34]; there it was concluded that the trend in crossphase was associated with a change in the dominant instability, from ion temperature gradient (ITG) or mixed ITG/TEM at low (more negative) values of α_{n_e,T_e} to dominant TEM at higher values. In those experiments, ECH was added near the axis of Ohmic and NBI-heated L-mode plasmas, which had large effects on T_e/T_i and collisionality, but caused a comparatively small change to $L_{T_e}^{-1}$. Here, with targeted off-axis ECH, large changes to $L_{T_e}^{-1}$ were induced. Either set of parameter changes would be expected to favor TEM instability.

Three direct measurements of turbulence characteristics are individually consistent with ∇T_e-driven trapped electron modes at high $L_{T_e}^{-1}$: $L_{T_e}^{-1}$ threshold, convergence of α_{n_e,T_e} at high $L_{T_e}^{-1}$, and the $(\delta T_e/T_e)/(\delta n/n)$ trend. The collisionality and β reside in a TEM relevant regime. Both the mean linear growth rates and $\delta T_e/T_e$ showing a sharp increase at $\eta_e \approx 2$ further supports the ∇T_e-TEM interpretation. In sensitivity studies, the growth rates for the electron direction propagating modes in Fig. 3(a) increase with $L_{T_e}^{-1}$ and are stabilized by increasing $\nu_{ei}/(c_s/a)$, which identifies the modes in the calculation as ∇T_e-TEM. The accumulated evidence strongly enforces the identification of the experimentally observed threshold with ∇T_e-TEM turbulence.

It is notable that while $\widetilde{Q}_e/(n_e T_e)$ increases by more than 10×, $\delta T_e/T_e$ only increases by

$\sim 2\times$. The electrostatic turbulent cross-field electron heat flux can be written as[36]

$$\widetilde{Q}_e = \frac{3n_eT_e}{2B}\sum_{k_\theta} k_\theta \left(\frac{|\delta n_e|}{n_e}|\delta\varphi|\gamma_{n_e,\varphi}\sin\alpha_{n_e,\varphi} + \frac{|\delta T_e|}{T_e}|\delta\varphi|\gamma_{T_e,\varphi}\sin\alpha_{T_e,\varphi} \right), \tag{2}$$

where the sum is taken over the fluctuations associated with each k_θ and φ is the electrostatic potential (which is not measured). Nonlinear gyrokinetic simulations of similar plasmas found that the conductive term $(\delta T_e, \delta\varphi)$ dominated, accounting for $\sim 90\%$ of $\widetilde{Q}_e$[37]. The α_{n_e,T_e} measurements indicate a more subtle picture than the $\delta T_e/T_e$ measurements alone. Changes to α_{n_e,T_e} give reason to consider that the transport related crossphases, $\alpha_{n_e,\varphi}$ and $\alpha_{T_e,\varphi}$, might also change in such a way that the turbulent heat flux increases. Other possibilities include additional transport from higher k_θ's than are measured (in past work from DIII-D high-k density fluctuations, $k_r \sim 35$ cm^{-1}, did increase[34] and intermediate-k density fluctuations, $k_\theta \sim 4$ and 8 cm^{-1}, did change[35]), a modification to the average wavenumber of the low-k fluctuations, and non-local transport.

Two plausibility checks on the role of crossphase modifications can be accomplished briefly (taking high-k and other contributions to be negligible). First, by contradiction, if one assesses only the conductive term and assumes that the coherency and crossphases between fluctuations *do not change*, then $\tilde{\varphi}$ would have to increase by $\sim 5\times$. One would expect such a change to be reflected in the particle transport (unless $\sin\alpha_{n_e,\varphi} \approx 0$), which was not the case. Second, the required potential fluctuations to drive the observed $\widetilde{Q}_e/(n_eT_e)$ can be assessed. At high $L_{T_e}^{-1}$, $\widetilde{Q}_e/(n_eT_e) \approx 45$ m/s and $\delta T_e/T_e \approx 2\%$. To set a bound, take $\gamma_{T_e,\varphi} = 1$ and $\alpha_{T_e,\varphi} = 90°$. Also take the average poloidal wavenumber to be $\langle k_\theta \rangle = 1.5$ cm^{-1} ($k_\theta\rho_s \approx 0.3$). One then finds that for the conductive term to account for $\widetilde{Q}_e/(n_eT_e) = 45$ m/s at low-k would require $e\tilde{\varphi}/T_e \approx 2.5\%$, a level similar to the measured $\delta T_e/T_e$—the conclusion being it is indeed plausible.

We have reported the first observation of a critical gradient threshold for a measured turbulent fluctuation level in the core of a tokamak. Both analysis of electron thermal transport and measurements of electron temperature fluctuations show a critical threshold

in L_{Te}^{-1} and little sensitivity to rotation or rotation shear. Measurements and supporting calculations strongly constrain identifying the mode responsible for the observed critical gradient threshold to the ∇T_e-TEM instability. The clear inference is that the $\delta T_e/T_e$ increase from ∇T_e-driven TEM turbulence plays a causal role for the increased transport and stiffness.

This work supported in part by the U.S. Department of Energy under DE-FG03-01ER54615, DE-FG02-08ER54984, DE-FC02-04ER54698, DE-FG02-95ER54309, DE-FG02-89ER53296, DE-FG02-08ER54999, DE-FG02-06ER54871, DE-FG02-07ER54917, and DE-FC02-93ER54186.

REFERENCES

[1]G. G. Howes *et al.*, Astrophys. J. **651**, 590 (2006)

[2]P. Fauchais, J. Phys. D: Appl. Phys. **37**, R86 (2004)

[3]G. R. Tynan *et al.*, Plasma Phys. Controlled Fusion **51**, 113001 (2009)

[4]S. Grossman, Rev. Mod. Phys. **72**, 603 (2000)

[5]W. Horton, Rev. Mod. Phys. **71**, 735 (1999)

[6]P. Deschamps *et al.*, Phys. Rev. Lett. **31**, 1457 (1973)

[7]A. K. Sen *et al.*, Phys. Rev. Lett. **66**, 429 (1991)

[8]X. Wei *et al.*, Phys. Plasmas **17**, 042108 (2010)

[9]G. T. Hoang *et al.*, Phys. Rev. Lett. **87**, 125001 (2001)

[10]D. R. Baker *et al.*, Phys. Plasmas **8**, 4128 (2001)

[11]F. Ryter *et al.*, Phys. Rev. Lett. **95**, 085001 (2005)

[12]Y. Camenen *et al.*, Plasma Phys. Controlled Fusion **47**, 1971 (2005)

[13]P. Mantica *et al.*, Phys. Rev. Lett. **102**, 175002 (2009)

[14]P. Bak *et al.*, Phys. Rev. Lett. **59**, 381 (1987)

[15]B. A. Carreras *et al.*, Phys. Plasmas **3**, 2903 (1996)

[16]J. E. Kinsey *et al.*, Nucl. Fusion **51**, 083001 (2011)

[17]For consistency with Ref. 19 the definition used for all scale lengths is $L_j^{-1} = \rho_{max}^{-1} j^{-1} \partial j / \partial \rho$; the radial coordinate, ρ, is the square root of the normalized toroidal flux and $\rho_{max} = \sqrt{\Phi/(\pi B_0)}$, where Φ is the toroidal flux within the last closed flux surface. For the plasmas reported on here $\rho_{max} \approx 79$ cm.

[18]J. Luxon, Nucl. Fusion **42**, 614 (2002)

[19]J. C. DeBoo *et al.*, Phys. Plasmas **19**, 082518 (2012)

[20]M. Häse *et al.*, Rev. Sci. Instrum **70**, 1014 (1999)

[21]A. E. White *et al.*, Phys. Plasmas **17**, 056103 (2010)

[22]J. C. Hillesheim *et al.*, Rev. Sci. Instrum. **81**, 10D907 (2010)

[23]A. E. White *et al.*, Rev. Sci. Instrum. **79**, 103505 (2008)

[24]J. C. Hillesheim *et al.*, Rev. Sci. Instrum. **80**, 083507 (2009)

[25]G. R. McKee *et al.*, Rev. Sci. Instrum. **70**, 913 (1999)

[26]G. Cima *et al.*, Phys. Plasmas **2**, 720 (1995)

[27]B.B. Kadomtsev *et al.*, Nucl. Fusion **11**, 67 (1971)

[28]A. E. White *et al.*, Phys. Plasmas **17**, 020701 (2010)

[29]F. Imbeaux *et al.*, Plasma Phys. Control. Fusion **44**, 1425 (2002)

[30]T. Dannert and F. Jenko, Phys. Plasmas **12**, 072309 (2005)

[31]D.R. Ernst *et al.*, Phys. Plasmas **16**, 055906 (2009)

[32]G. M. Staebler *et al.*, Phys. Plasmas **12**, 102508 (2005)

[33]T. L. Rhodes *et al.*, Nucl. Fusion **51**, 063022 (2011)

[34]G. Wang *et al.*, Phys. Plasmas **18**, 082504 (2011)

[35]J. C. DeBoo *et al.*, Phys. Plasmas **17**, 056105 (2010)

[36]A. J. Wootton *et al.*, Phys. Fluids B **2**, 2879 (1990)

[37]C. Holland *et al.*, Nucl. Fusion **52**, 063028 (2012)

FIGURE CAPTIONS

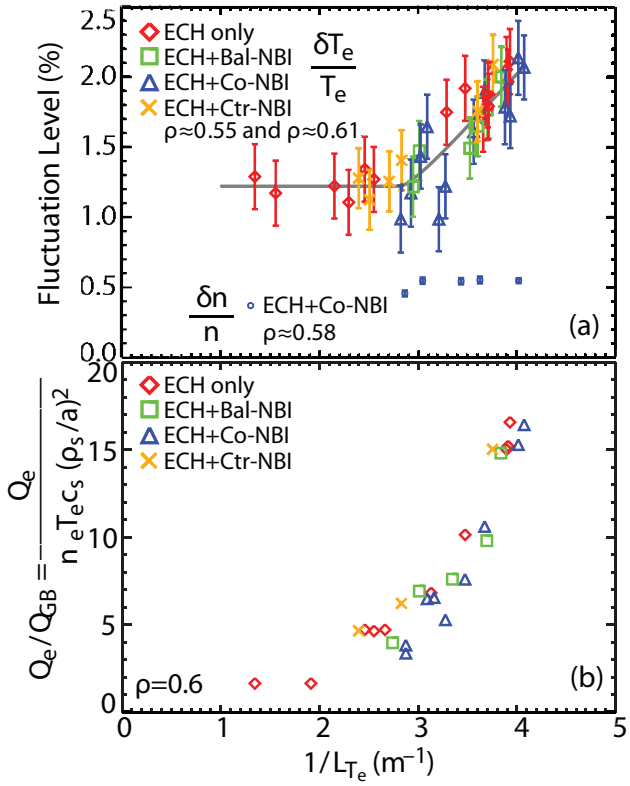

Fig. 1, J.C. Hillesheim, Phys. Rev. Lett.
(Color online)

FIG. 1. (Color online) (a) Electron temperature and density fluctuations and (b) electron heat flux at $\rho = 0.6$ inferred from transport analysis as a function of $|\nabla T_e|/T_e$. The critical gradient for $\delta T_e/T_e$ was determined to be $L_{T_e}^{-1}|_{crit} = 2.8 \pm 0.4$ m^{-1}.

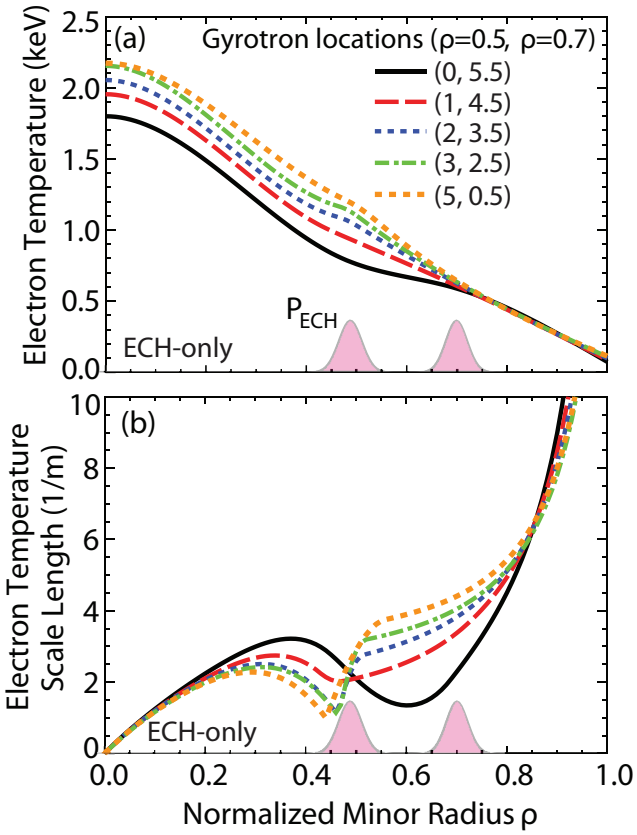

Fig. 2, J.C. Hillesheim, Phys. Rev. Lett.
(Color online)

FIG. 2. (Color online) Response of (a) electron temperature profile and (b) inverse scale length profile to ECH location for ECH-only case. ECH power deposition profiles are annotated. Legend indicates number of ECH gyrotrons resonant at $\rho = 0.5$ and $\rho = 0.7$, with fractional gyrotrons for the modulated source.

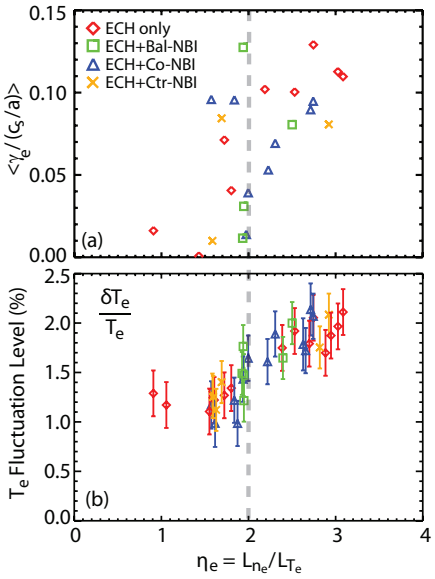

Fig. 3, J.C. Hillesheim, Phys. Rev. Lett.
(Color online)

FIG. 3. (Color online) (a) Linear gyrofluid growth rates of fastest growing modes propagating in the electron diamagnetic direction averaged over $0.0 \leq k_\theta \rho_s \leq 0.4$ and (b) electron temperature fluctuations as a function of $\eta_e = L_{n_e}/L_{T_e}$. Dashed vertical lines for reference at $\eta_e = 2$.

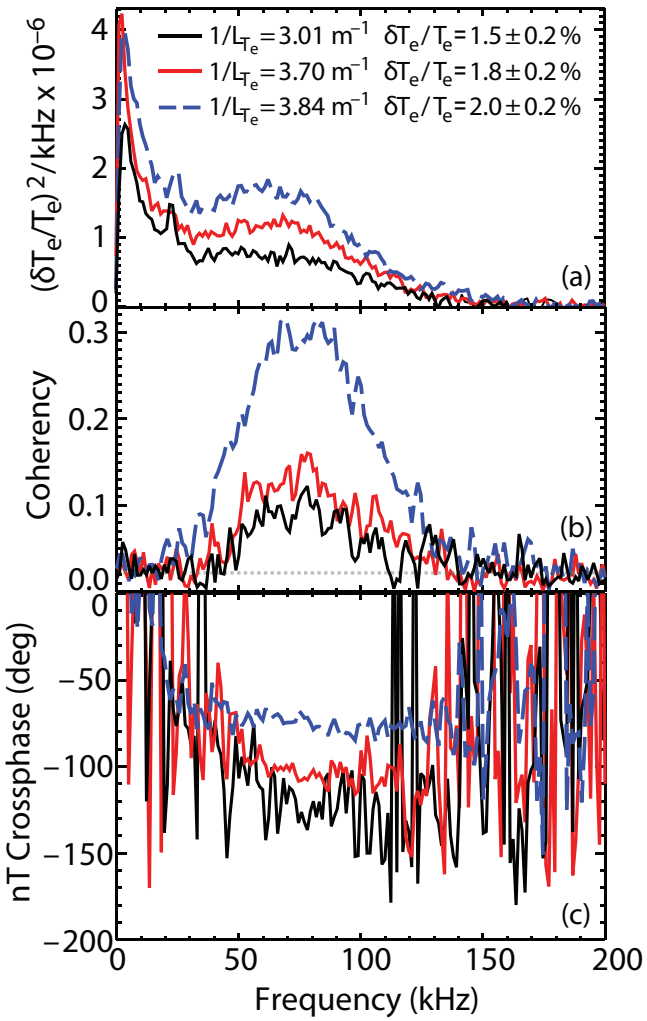

Fig. 4, J.C. Hillesheim, Phys. Rev. Lett.
(Color online) blue 10 & 3 pt

FIG. 4. (Color online) (a) Electron temperature fluctuation power spectra. (b) Coherency and (c) crossphase between CECE and reflectometry for ECH+Bal-NBI at $\rho \approx 0.6$. Legend indicates local values of $L_{T_e}^{-1}$ for the measurements and integrated (0-400 kHz) values of $\delta T_e/T_e$. Approximate coherency noise floor shown by dashed horizontal line in (b).

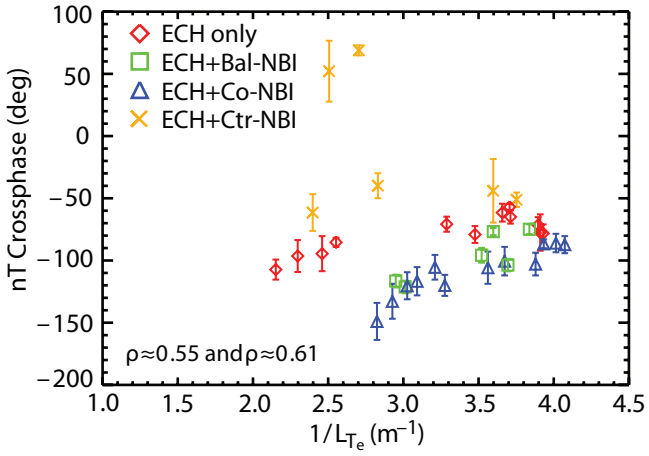

Fig. 5, J.C. Hillesheim, Phys. Rev. Lett.
(Color online)

FIG. 5. (Color online) Crossphase angle between electron density and temperature fluctuations.